

# Active beam steering enabled by photonic crystal surface emitting laser

Jiahao Si

*Laboratory of Solid State Optoelectronics Information Technology,  
Institute of Semiconductors, CAS,  
Beijing, China  
sijiahao@semi.ac.cn*

Yuanbo Xu

*Laboratory of Solid State Optoelectronics Information Technology,  
Institute of Semiconductors, CAS,  
Beijing, China  
ybxu@semi.ac.cn*

Wenzhen Liu

*Laboratory of Solid State Optoelectronics Information Technology,  
Institute of Semiconductors, CAS,  
Beijing, China  
wenzhenliu@semi.ac.cn*

Mingjin Wang

*Laboratory of Solid State Optoelectronics Information Technology,  
State Key Laboratory on  
Integrated Optoelectronics,  
Institute of Semiconductors, CAS,  
Beijing, China  
mingjinwang@semi.ac.cn*

Jingxuan Chen

*Laboratory of Solid State Optoelectronics Information Technology,  
Institute of Semiconductors, CAS,  
Beijing, China  
chenjx@semi.ac.cn*

Zihao Chen

*State Key Laboratory of Advanced Optical Communication Systems and Networks,  
Department of Electronics & Frontiers Science Center for Nano-optoelectronics,  
Peking University,  
Beijing, China  
zihao.chen@pku.edu.cn*

Zheng Zhang

*Huawei Technologies Co. Ltd.,  
Wuhan, China  
zhangzheng19@huawei.com*

Wanhua Zheng

*Laboratory of Solid State Optoelectronics Information Technology,  
State Key Laboratory on  
Integrated Optoelectronics,  
Institute of Semiconductors, CAS,  
College of Future Technology,  
Center of Materials Science and  
Optoelectronics Engineering,  
University of Chinese Academy of Sciences,  
Beijing, China  
whzheng@semi.ac.cn*

**Abstract**—A dynamically controlled beam steering photonic crystals surface-emitting laser is proposed in this work. We demonstrate its fast beam steering across a range of  $3.2^\circ \times 4^\circ$  in a time scale of 500 nanoseconds.

**Keywords**—Active beam steering, Photonic crystals, Surface-emitting laser

## I. INTRODUCTION

Optical beam steering system is a key component of light detection and ranging (LiDAR) devices, which is in high demand due to the rise of autonomous driving technology. Passive systems which rely on external light sources dominate the current commercial beam steering methods. The unendurable loss of light and the difficulty of miniaturization hinder the practical applications of passive beam steering technology. Borrowing from the concept of active electronically scanned array radars in radio-frequency spectrum [1] and directional

beam emissions of composite photonic-crystal (PhC) lasers [2], [3], active optical beam steering is proposed. This method shows great potential in on-chip integration and low-loss power emission.

In this work, a novel method for active beam steering utilizing a photonic-crystal surface-emitting laser (PCSEL) is proposed and experimentally demonstrated. By confining the volume of light into tens-of-wavelengths scale in all three directions, the continuous band is quantized into discrete optical modes in k space. With different currents injected into multiple quantum wells (MQWs), the peak of optical gain shifts, thereby exciting different modes that exhibit quantized momentum and directional emission. Thus, with changing the current of the laser, we can dynamically control the emitting direction of the PCSEL to realize fast active beam scanning. In our prototype device, the switch rate up to 1 MHz across a range of  $3.2^\circ \times 4^\circ$  is available.

Corresponding Author: Chao Peng & Wanhua Zheng

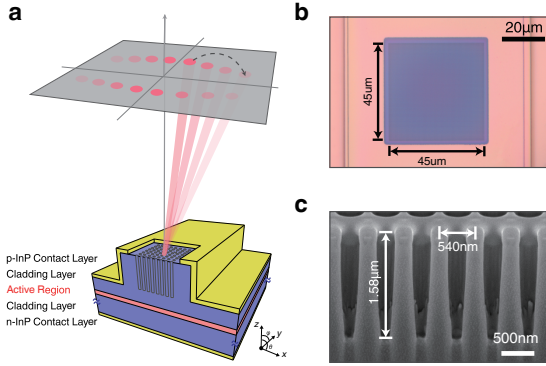


Fig. 1. Structure of the active beam steering PCSEL. (a) The schematic of the PCSEL. (b, c) The top view and the slitting view of the PhC by optical microscope and scanning electron microscope respectively.

## II. DESIGN AND PRINCIPLES

Fig. 1a shows the schematic view of our design. The PhC with the depth  $h = 1580$  nm are patterned on a ridge which is  $1.8 \mu\text{m}$  wide and  $90 \mu\text{m}$  high. The PhC structure in size of  $45 \times 45 \mu\text{m}^2$  consists of  $84 \times 84$  air-holes. The top and bottom surfaces of the PCSEL are covered with metals. A window is left at the top of the ridge by lift-off process to emit the laser. The active layers are AlGaInAs MQWs at the center of the wafer. With a periodicity of  $540$  nm and a radius of  $167$  nm, our device operates at an eye-safe wavelength around  $1550$  nm. Because of the coated metal, the boundaries of PhC in  $x$  directions are perfectly reflective and partly reflective in  $y$  direction. Notably, in comparison to other reported PCESLs [4], [5], our device features air-holes located on the upper surface rather than being buried within the wafer. The elimination of the sophisticated re-growth process represents that the manufacturing process is substantially simplified. The top view of the device is shown in Fig. 1b with optical microscope, and the slitting diagram of PhC is shown in Fig. 1c with the scanning electron microscope.

We calculate the TE mode photonic band of PhC with infinite periodic periodicity. In our design, the modes in the vicinity of the second-order  $\Gamma$  are excited. There are four bands tagged as TE-A to D at the second-order  $\Gamma$  point. TE-A is selected to be excited due to its relative high quality factor. Because of the reflective in horizontal directions, the light is confined into a small volume. Therefore, the band is quantized into discrete modes, distributed at integer multiples of  $\frac{\pi}{L}$  in  $k$  space.  $L$  is the length of PhC area. A set of the integer  $(p, q)$  is used to describe the mode in  $(p\frac{\pi}{L}, q\frac{\pi}{L})$  (Fig. 2a). Along the  $z$  direction, due to the mirror of metals in the bottom, the confinement of light in the vertical direction is still present. The envelop of electric field folds several times in our calculation, as shown in Fig. 2b, which can be represent by an integer  $m$ . Therefore, the optical modes are discrete in momentum space, labeled by  $(m, p, q)$  (Fig. 3). The near-field and far-field patterns of three selected modes, U(8, 3, 6), V(11, 4, 7), and W(13, 5, 8), are computed and plotted by the

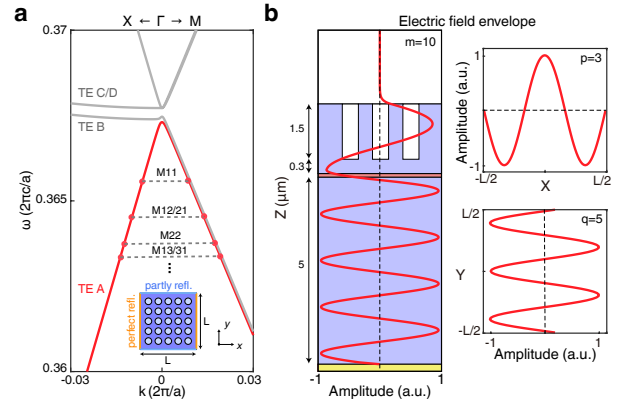


Fig. 2. Quantized mode. (a) Discrete TE photonic band around the second order  $\Gamma$  point in transverse directions. (b) The envelop of electric field in all directions, labeled by  $(m, p, q)$ .

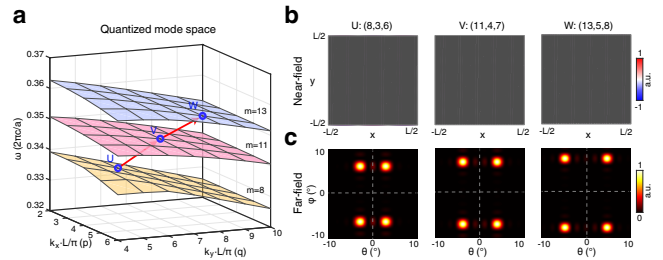


Fig. 3. Examples of the discrete modes. (a) A schematic of band TE-A in 3D momentum space. (b,c) Near-fields and Far-fields of U(8, 3, 6), V(11, 4, 7), and W(13, 5, 8).

Couple Wave Theory(CWT) [6] method, which demonstrates that the emitting angle changes with the switch of modes.

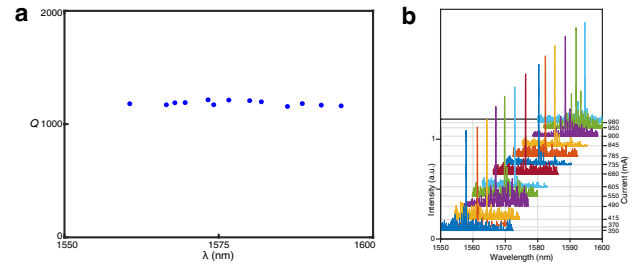


Fig. 4. (a) The passive Q factors of the modes in telecom-wavelength range. (b) The shifting of the gain peak in the PCSEL.

The passive quality factors of various telecommunication wavelength modes are calculated, with no consideration of material gain or loss (Fig. 4a). The boundaries in  $x$  direction are assumed to have the reflectivity of 1.0 and 0.8 in  $y$  direction. It can be observed that the Q factors are similar, around 1000, which implies the selection of the lasing mode only depends on gain of materials rather than Q factors. We measure the shift of gain peak in a PCSEL sample (Fig. 4b). With the increasing of injecting currents, the center of the

gain changes, and modes with different emitting directions are excited. So we can control the direction of emission by varying the injection current.

### III. RESULT AND DISCUSSION

#### A. Laser Behaviors

First, we test the PCSEL sample to investigate the effects of current variation on its emission direction (Fig. 5a). The experimental results are in agreement with the theoretical predictions of CWT method. As illustrated in Fig. 5d, the lasing mode exhibits a zigzag motion in the discrete momentum space. When the current increasing from 350 mA to 980 mA, the emission angle ( $\theta, \phi$ ) shown in far-field pattern moves from  $2.9^\circ \times 18.6^\circ$  to  $6.1^\circ \times 14.6^\circ$ , exhibiting a  $3.2^\circ \times 4^\circ$  2D scanning. And our device operates in a single mode at 980 mA with the linewidth of 1.8 MHz.

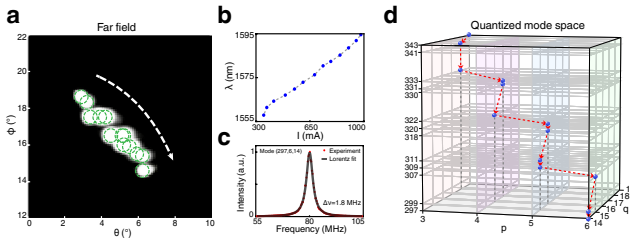


Fig. 5. The active beam steering behavior. (a) The far field in first quadrants when currents increase from 350 mA to 980 mA. (b) The gain peak wavelengths with different currents. (c) The linewidth at the current of 980 mA measured by delayed self-heterodyne method. (d) The modes change with different injecting current in 3D quantized momentum space.

#### B. Speed Evaluation of active beam steering of the PCSEL

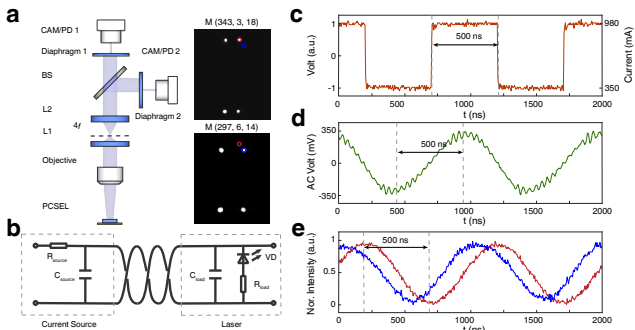


Fig. 6. Switch speed of active beam steering PCSEL. (a) Schematic of our experimental design. BS: beam-splitter; L: lens; PD: photo-diode; CAM: camera. (b) The driver circuit model of the laser. (c) The 1 MHz electric bipolar waveform to switch injecting currents. (d) The AC voltage measured at the electrodes of the laser. (e) The normalized optical intensity of the two modes, showing the switching time between two modes is approximately 500 ns.

Then we characterize the speed of active beam steering of the PCSEL. A pair of modes, (343, 3, 18) at 350 mA and (297, 6, 14) at 980 mA are selected. Diaphragms with pinholes are used to filter and isolate the emitting light beam

spots of two selected modes in the first quadrant. Meanwhile, two photo-diodes (PDs) are used to detect beam spots. An electrical bipolar waveform with a frequency of 1 MHz is applied to the PCSEL to achieve current switching. Due to the bandwidth of the current source, the voltage actually loaded on the device is sinusoidal in shape. The intensity of the two spots peaks reaches the peak in turn within a time scale of 500 ns, indicating that our device can achieve fast beam steering scan.

The above experiments demonstrate a new active beam steering method which can realize fast scanning. In order to adapt the need of practical applications such as LiDAR, our design can be further optimized in many aspects, including divergence angle, scanning step, range and speed. By increasing the device footprint further beyond  $45 \times 45 \mu\text{m}^2$ , it is possible to achieve smoother scanning step, lower divergence angle and higher power. Additionally, the range of the scan mainly depends on dispersion of the band. By introducing a super-cell structure, it is possible to design a flatter band, which enables an expanded scanning range with the same gain frequency shifting. Noteworthy, as a prototype, the parameters of our design, such as the metal contacts, ridge geometry and MQWs layer, do not optimize for a faster scan speed. Therefore, active beam steering technology exhibits significant potential for further development and optimization.

### IV. CONCLUSION

We propose a new method of active beam steering in this work. Without passive steering structure, a single PCSEL can realize directional control of the light emission through current modulation. Our prototype device demonstrates a performance with a linewidth in megahertz scale, emitting power of 10 mW, and scan range of  $3.2^\circ \times 4^\circ$  in a switch time of 500 ns. This technology provides new possibilities for applications such as laser processing [7], laser sensor [8], and optical communication [9].

### ACKNOWLEDGMENT

This work was partly supported by the National Key Research and Development Program of China (2021YFB2801400), the National Natural Science Foundation of China (61922004, 62135001, and 62205328), National Key Research and Development Program of China (2020YFB1806405), the Major Key Project of PCL (PCL2021A14), and Huawei Technologies Co. Ltd. Grant TC20220323035 on the lasers. The simulation of this work was supported by High-performance Computing Platform of Peking University.

### REFERENCES

- [1] H. T. Friis and C. B. Feldman, ‘A multiple unit steerable antenna for short-wave reception’, Proc. Inst. Radio Eng., vol. 25, no. 7, pp. 841–917, Jul. 1937.
- [2] Y. Kurokawa et al., ‘On-chip beam-steering photonic-crystal lasers’, Nature Photon, vol. 4, no. 7, Art. no. 7, Jul. 2010.
- [3] R. Sakata et al., ‘Dually modulated photonic crystals enabling high-power high-beam-quality two-dimensional beam scanning lasers’, Nat Commun, vol. 11, no. 1, p. 3487, Dec. 2020.

- [4] K. Hirose, Y. Liang, Y. Kurosaka, A. Watanabe, T. Sugiyama, and S. Noda, ‘Watt-class high-power, high-beam-quality photonic-crystal lasers’, *Nature Photon*, vol. 8, no. 5, Art. no. 5, May 2014.
- [5] M. Yoshida et al., ‘Double-lattice photonic-crystal resonators enabling high-brightness semiconductor lasers with symmetric narrow-divergence beams’, *Nature Mater*, vol. 18, no. 2, pp. 121–128, Feb. 2019.
- [6] Y. Liang, C. Peng, K. Sakai, S. Iwahashi, and S. Noda, ‘Three-dimensional coupled-wave analysis for square-lattice photonic crystal surface emitting lasers with transverse-electric polarization: finite-size effects’, *Opt. Express, OE*, vol. 20, no. 14, pp. 15945–15961, Jul. 2012.
- [7] P. V. Braun and M. L. Brongersma, ‘Photochemistry democratizes 3D nanoprinting’, *Nat. Photonics*, vol. 15, no. 12, pp. 871–873, Dec. 2021.
- [8] D. J. Lum, ‘Ultrafast time-of-flight 3D LiDAR’, *Nat. Photonics*, vol. 14, no. 1, pp. 2–4, Jan. 2020.
- [9] I. I. Smalyukh, Y. Lansac, N. A. Clark, and R. P. Trivedi, ‘Three-dimensional structure and multistable optical switching of triple-twisted particle-like excitations in anisotropic fluids’, *Nature Mater*, vol. 9, no. 2, Art. no. 2, Feb. 2010.